ELSEVIER

International Journal of Heat and Fluid Flow 20 (1999) 492–498

International Journal of HEAT AND FLUID FLOW

www.elsevier.com/locate/ijhff

Contribution to droplet breakup analysis

P. Berthoumieu *, H. Carentz, P. Villedieu, G. Lavergne

ONERA, Centre de Toulouse, 2 Avenue Edouard Belin, BP 4025, 31055 Toulouse, France

Abstract

A basic experiment has been developed to investigate the secondary breakup of droplets in high velocity airstreams. Monosized droplets are injected in the mixing layer of two co-flowing airflows. Various conditions have been tested, different initial drop sizes, different air and droplet velocities to evaluate the influence of the Weber number on breakup regimes. An image processing technique has been developed to measure droplet diameter. Comparisons with numerical simulation conclude this work.

Notation

t_b	breakup time
D_g	droplet diameter
C_d	drag coefficient
ρ_g	gas density
Lp	Laplace number
ρ_l	liquid density
μ_l	liquid viscosity
Oh	Ohnesorge number
Re_p	particle Reynolds number
σ	surface tension
C	spacing parameter
ΔV	velocity differential (air–droplet)
We	Weber number

1. Introduction

The propulsion engines performance is conditioned by the delay of fuel evaporation, which is directly influenced by the distribution of droplet size. The smaller the droplet diameters, the shorter is the evaporation time and the better is the combustion. So each phenomenon which leads to droplet diameter reduction is of primary importance in engine propulsion design. The effects of airflow on droplets have been studied for a long time (Lenard, 1904). Works in literature show that deformation and droplets breakup are depending on boundary conditions of the liquid gas interface. The main factors are:

- Droplet acceleration,
- Pressure, temperature, density and viscosity of the two phases,
- Surface tension.

A dimensional analysis of those factors shows the importance of the Weber and the Ohnesorge numbers:

$$\mathrm{We} = \frac{\rho_g \Delta V^2 D_g}{\sigma}, \qquad \mathrm{Oh} = \frac{\mu_l}{\sqrt{\rho_l D_g \sigma}}.$$

Krzeczkowski (1980), Pilch and Erdman (1987), Hsiang and Faeth (1992) and Shraiber et al. (1996) give a classification of breakup regimes as functions of these numbers.

Many of those studies consider the interaction between shock wave and droplet fallen due to gravity (Hsiang and Faeth, 1995, Wierzba, 1990). This kind of experiments produce a "clean" breakup (axisymmetrical bag breakup for example) which is not met in a combustion chamber.

The purpose of this paper is to build an experiment representative of a combustion chamber condition, air flow with shearing and to compare experimental data with a numerical simulation. Droplet size is measured along the airflow to obtain the evolution of the PDF of droplet sizes.

2. Experimental set-up

A vibrating orifice is used to generate a stream of monosized droplets in an air stream. As it can be seen Fig. 1 two airflows are supplied by two ducts. Droplets are injected in the mixing layer of the two flows.

Two kinds of measurements have been undertaken:

- Aerodynamic characterization by hot wire.
- Visualization and image processing for the dispersed phase characterization.

3. Visualization and image processing

3.1. Particle sizing

Generally a Phase Doppler Particle Analyzer (PDPA) is used for droplet size measurement but in this case this technique could not be applied. PDPA can only perform measurement on spherical particles. Due to the effects of the air stream initially spherical drops are deformed (Fig. 2). So, an

* Corresponding author. E-mail: berthoumieu@onecert.fr

0142-727X/99/$ – see front matter
PII: S0142-727X(99)00037-5

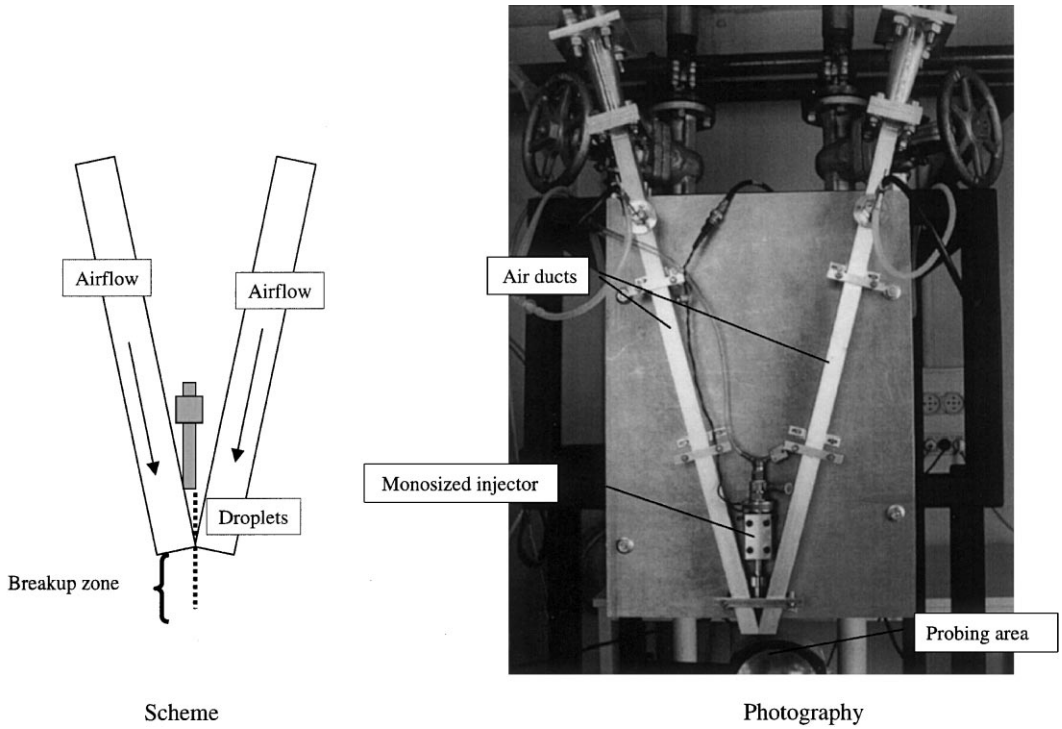

Fig. 1. Experimental configuration.

image-processing technique was developed to perform size measurements.

A back lighting technique is applied to visualize the drops, which appear dark on a white background. A stroboscopic light freezes the droplet motion. Images are processed as follows (Fig. 3). First, a background image without droplets is memorized to take into account non-homogeneous lighting. Each recorded image is inverted to see droplets in white on a dark background, then the inverted background is subtracted from the initial image. At that time the droplets appears clear on a dark background. Assuming the droplets could be detected by their luminance level a threshold is applied on this image to obtain a binary image in which droplets appear in white. Then the surface of each white blob is measured; a scale factor gives the true surface. An equivalent diameter is calculated assuming that the droplets are spherical. The relative position of the centre of gravity is also measured to analyze the particle size as function of distance from the injection point.

A comparison was made with PDPA measurements in a zone where droplets are spherical, at 20 mm from the injection point. Fig. 4 shows comparative histograms. This comparison was made on about a thousand images.

A compromise must be found between the smallest droplet observation and the size of the field of view. The chosen limitation was to take into account drops with a diameter bigger than 20 μm. This limitation is similar to the one imposed by PDPA where the range, for taking into account big droplets, is 16–570 μm. In those conditions the field of view was 4.3 mm × 3.2 mm which corresponds to an image resolution of 768 pixels on 576 lines. Each pixel represents 5.6 μm, so a 20 μm drop covers a surface of 10 pixels. It is obvious that an error on surface estimation has a big influence on diameter, 10% of accuracy on surface estimation gives 5% on diameter measurement. This influence is more significant on small droplets where 10% of the surface corresponds to only one pixel. Nevertheless, small droplets represent a small part of the

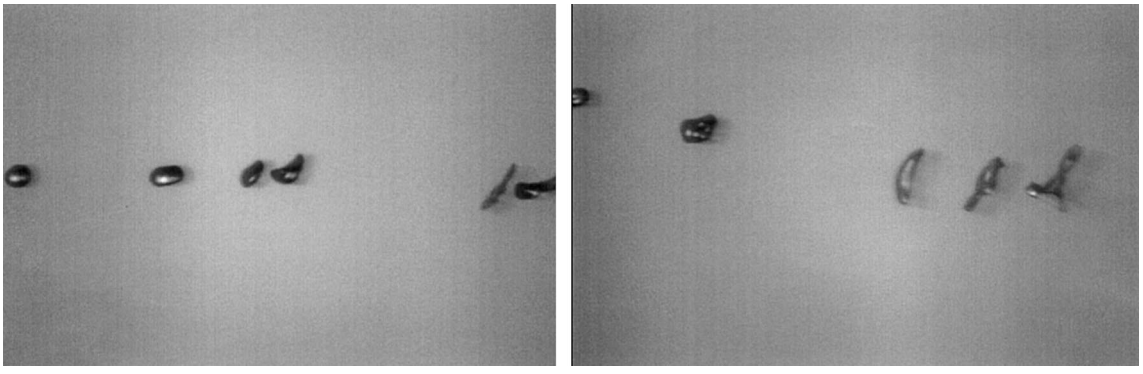

Fig. 2. Droplet deformation.

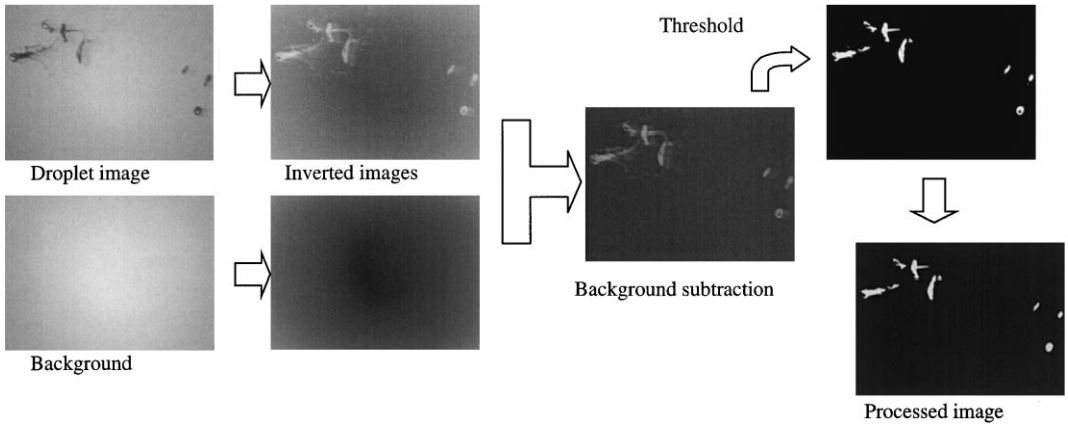

Fig. 3. Image processing.

injected liquid flow rate so this error has a little influence on mass flux.

3.2. Droplet repartition

By summation of binary images it is possible to create an image corresponding to the probability of droplet presence. Also the outline of this image gives the envelope of the jet expansion. This summation is done on 256 images.

4. Experimental results

Various experimental conditions have been tested for air velocities ranging from 20 to 80 m/s and a droplet velocity close to 10 m/s. Three median droplet sizes of 120, 220 and 320 μm have been injected. In all the cases, Weber number is less than 50, corresponding to the bag breakup conditions. Fig. 5. shows an example of breakup.

Fig. 6 shows an example of droplet deformation. The upper airflow velocity is 80 m/s and the lower one is 20 m/s. The complete field is about 20 cm, each view corresponds to 4.3 mm.

For size measurement this region is split in slices of 2 mm downstream the injection point. In each slice particles are measured and a size histogram is obtained. Fig. 7 shows, for each slice, the corresponding size histogram.

5. Numerical simulations

All the calculations have been performed using a Lagrangian code developed at ONERA. The breakup model was elaborated on the basis of correlation coming from the literature or experiments carried out at ONERA.

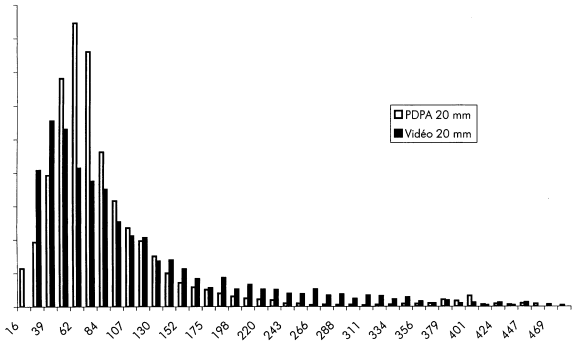

Fig. 4. Comparison between PDPA and video drop size measurement.

In the numerical simulation droplets are considered as spherical particles. Aerodynamic interaction between droplets is taken into account by using a drag coefficient depending of the distance between droplets. The drag coefficient is calculated with the following correlation build for high interaction droplets:

$$C_d = 53.2C^{0.6}\mathrm{Re}_p^{-1.524},$$

with C the spacing parameter (distance between droplets divided by droplets diameter), $2 \leqslant C \leqslant 40$ and Re_p the particle Reynolds number using droplet diameter and gas characteristics, $20 \leqslant \mathrm{Re}_p \leqslant 75$.

This correlation was obtained at ONERA by Adam (1997) using a monosized droplet generator.

Collision between droplets is not taken into account in the code. For the liquid phase, initial conditions are provided by experiments. The droplet initial size is that measured in the first slice near injection point. For the gas phase, the initial conditions are provided by a numerical simulation validated by hot wire measurements.

In the comparison with those experiments, three breakup regimes have been used according to a classification as the one proposed by Pilch and Erdman (1987): vibrational breakup, bag breakup and bag and stamen breakup. Breakup regime is identified by local Weber number value. Breakup occurs if the breakup time is reached. The formulation used for this delay was given by Nigmatulin (1990):

$$\frac{t_b}{t^*} = 6(1 + 1.2\ \mathrm{Lp}^{-0.37})(\mathrm{Log\ We})^{-0.25},$$

with: $t^* = (D_g/\Delta V)\left(\rho_l/\rho_g\right)^{0.5}$ and Laplace number: $\mathrm{Lp} = \rho_l \sigma D_g/\mu_l^2$.

In the first regime, the vibrational drop is broken in two random parts. Size is computed in order to obtain mass conservation. The relative position of each droplet depends on initial drop diameter; the expansion angle is also a random value less than 2.5°.

For the bag or bag and stamen regimes, the breakup process is similar but the number of droplets and their final position differ. Nigmatulin (1990) gives the value of 30% of the liquid mass corresponding to the bag volume which is evaporated in hot condition, as the experiment is in a cold flow condition there is no evaporation so the bag is considered to be split in 25–35 droplets. Those droplets are created at the initial position of the drop before breakup. As those drops are very small they are rapidly dispersed by the air stream. The ring

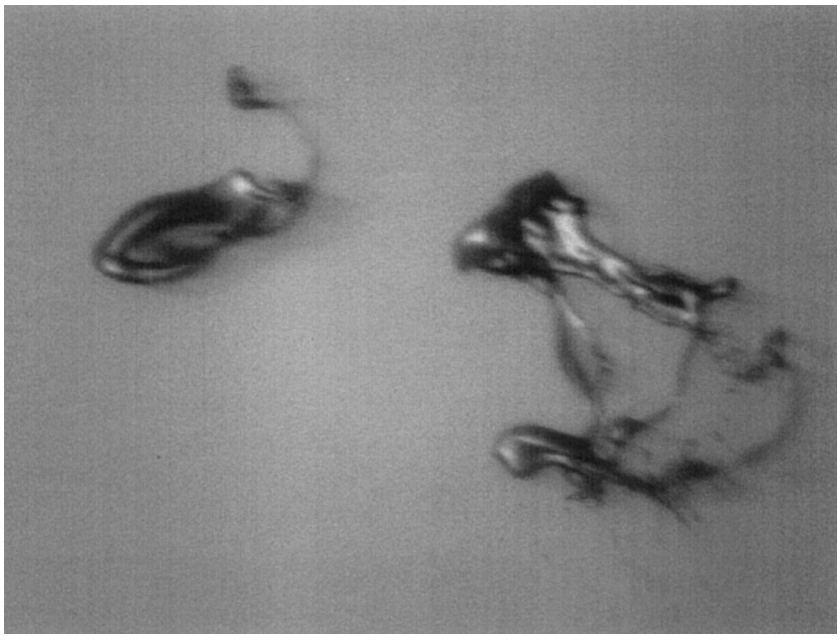

Fig. 5. Droplet bag breakup.

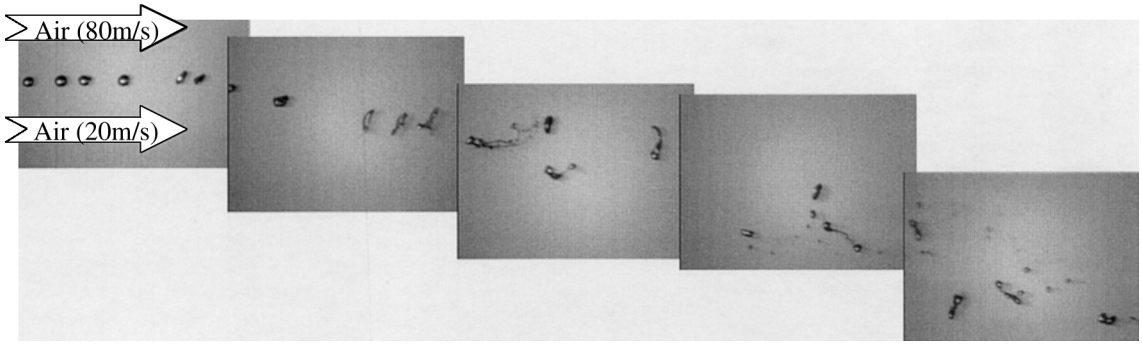

Fig. 6. Droplet deformation and breakup. Airflow velocity: 20 and 80 m/s. Initial drop size: 220 μm.

corresponding to 70% of the drop mass is split into 10–15 similar droplets. They are distributed on a circle with a radius equal to 4 times the initial drop radius. Expansion angle is lower than 7.5°. For stamen breakup 4–6 droplets are located on the ring axis.

For all regimes the drag coefficient varies during the breakup, due to the drop deformation. The velocity modification follows a correlation obtained by Hsiang and Faeth (1993),

$$\frac{U_0}{U} = 1 + 2.7\left\{\left(\frac{\rho_g}{\rho_l}\right)^{1/2}\frac{d_0}{d}\right\}^{2/3}.$$

In this correlation the dependence of the breakup regimes is taken into account by the maximal stable drop diameter d. U is the velocity after the breakup and variable suffix 0 are the initial drop characteristics.

Fig. 8 shows a superposition of experimental drop dispersion (gray level image and white outline or dashed line) and calculation (gray outline on plain line). Expansion angles are comparable in both cases; In the experiment a non-symmetric airflow velocity in the two air ducts could explain the upward movement of the measured limit compared with calculation outline.

The second comparison concerns size measurement. Initial droplet size repartition is given for computation. The comparison is made at 20 mm from the injection point. At this point it is assumed that secondary breakup is finished. The following histograms (Fig. 9) show (in black) the initial droplets repartition measured on the experiment and used for calculation, the two other histograms are obtained from measurement (white) and from calculation (gray). Those histograms have been normalized, for each class containing the maximum of droplets has the same value.

Air flow disturbs droplets injection and droplets approach each other and sometimes they collide and a new big droplet and some little one are created. This explains the shape of the initial histogram. In the computation all droplets are taken into account and there is no evaporation. In the experiment very small droplets are not detected, moreover droplets which are not in the field, blurred droplet images, give erroneous information. If contrast is not sufficient they don't enter in the counts. The model tested for bag breakup gives two classes of

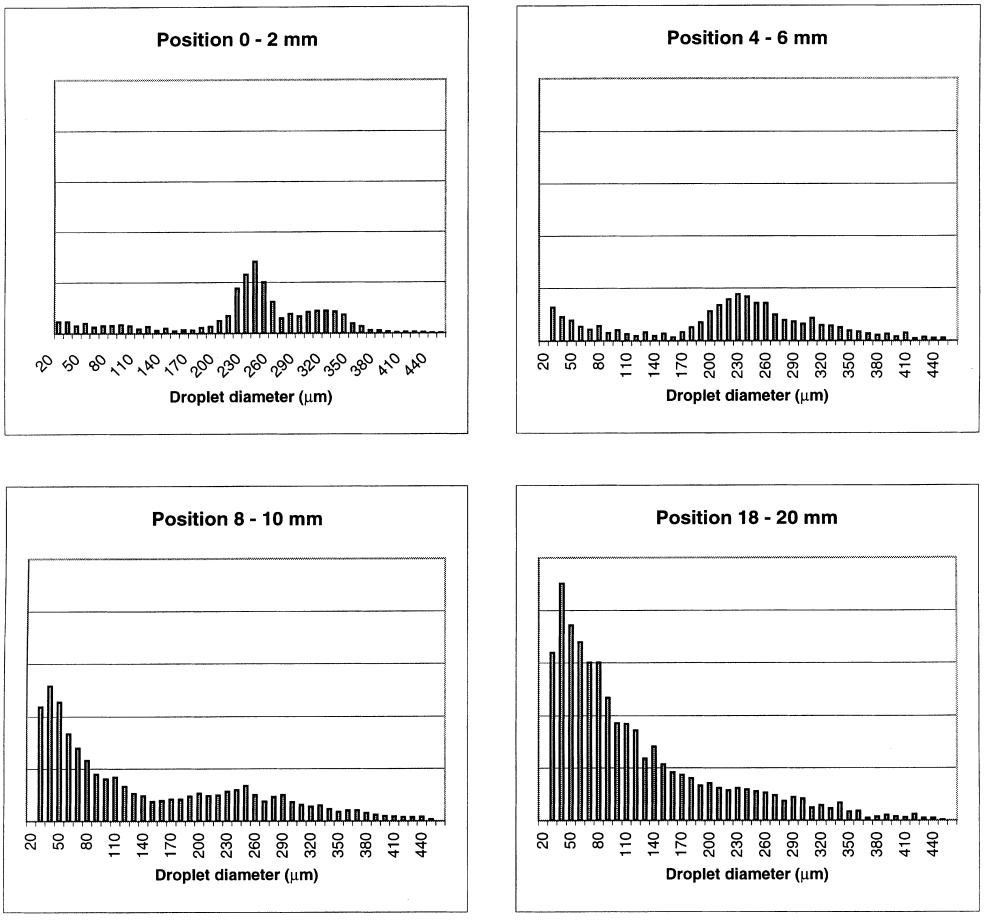

Fig. 7. Drop size evolution when moving away form injection point.

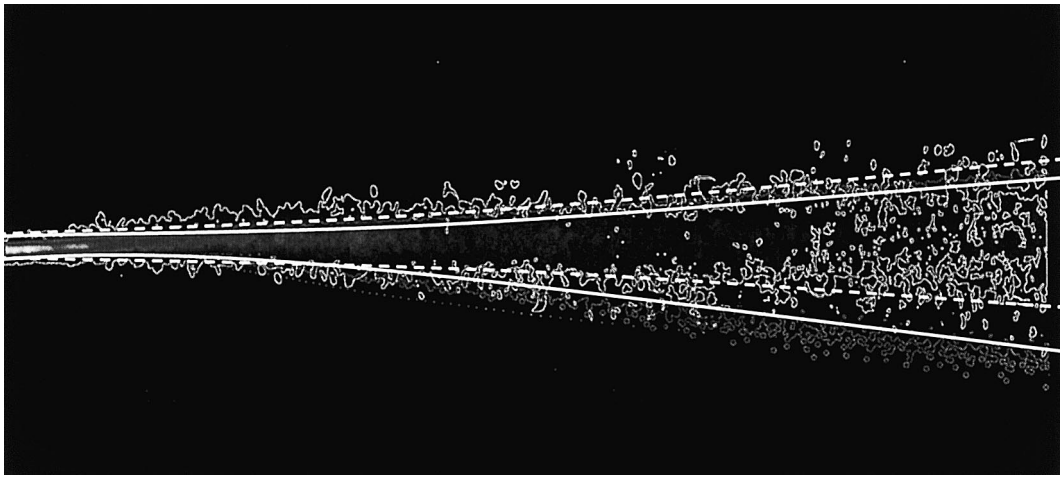

Fig. 8. Droplet repartition air velocity 60 m/s. Droplet diameter 220 μm.

sizes, the real breakup is more complex and gives a more continuous droplet size repartition.

6. Conclusion, perspectives

This basic experiment permits qualitative and quantitative visualizations of the breakup phenomenon. It appears that breakup is not so ideal as those proposed in the literature. The breakup is a continuous phenomenon and simulations like the one used give some interesting information but not completely the reality. Following the remarks on the droplet size repartition a new model is going to be implemented. First the duration of the fragmentation process is considered as a random variable following a Poisson's law. This means that during a time step Δt, the breakup probability for a given numerical drop is calculated as:

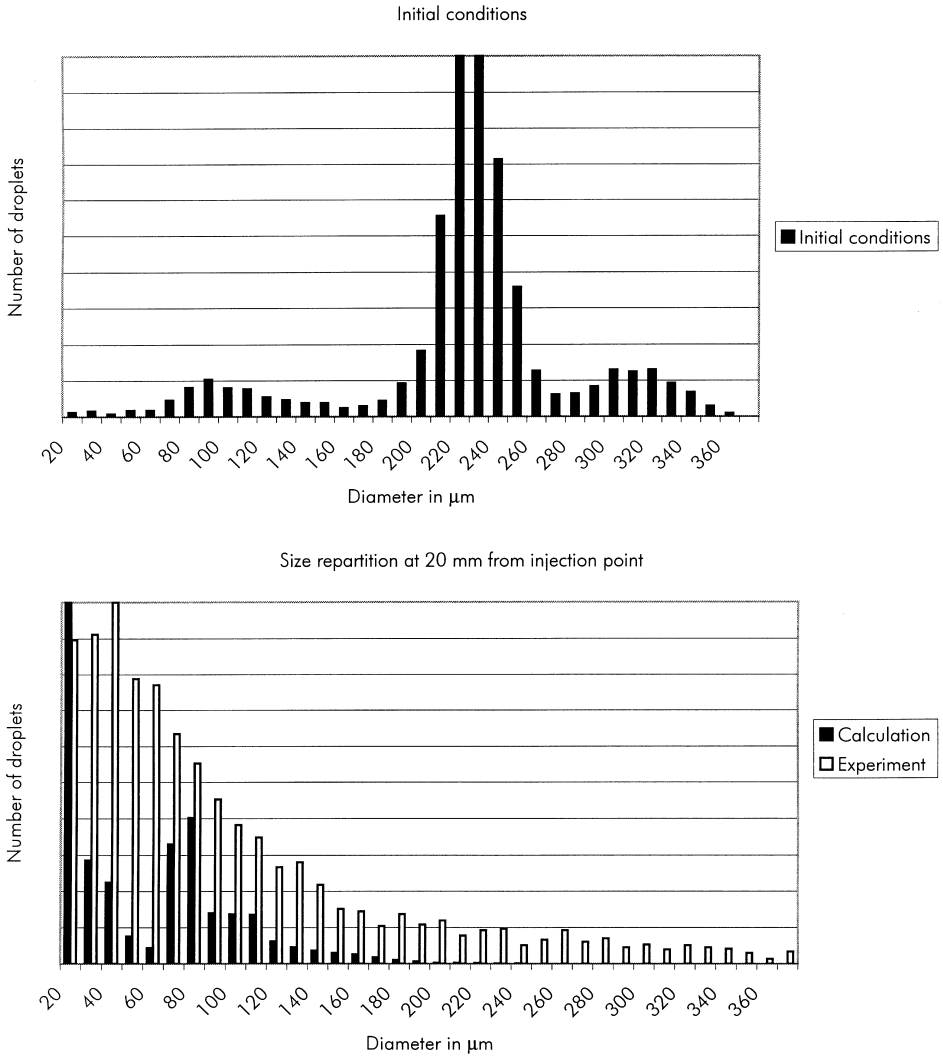

Fig. 9. Comparison of droplet size repartition, air flow 20 and 80 m/s.

$$P_{\text{bup}} = \begin{cases} 0 & \text{if } \text{We} < \text{We}_c, \\ \frac{\Delta t}{t_b} & \text{if } \text{We} \geqslant \text{We}_c, \end{cases}$$

where We_c is the critical Weber number and is approximately equal to 12. The fragment radius repartition function is supposed to obey to the following exponential law:

$$f(r) = \begin{cases} K \exp(-r/\bar{r}) & \text{if } r \leqslant r_{\max}, \\ 0 & \text{if } r > r_{\max}, \end{cases}$$

$r_{\max}$ is the maximum size of fragments and is given by the following experimental correlation:

$$r_{\max} = 2.1\text{We}^{-0.61} r_0,$$

where r_0 is the initial radius. The parameter $\bar{r}$ is calculated in order to respect a correlation on the mass median size (r_{mean}) of fragments. According to Pilch and Erdman (1987) we have:

$$r_{\text{mean}} = \frac{1}{2} r_{\max}.$$

Finally the constant K is adjusted in order to ensure the mass conservation.

$$K \int_0^{r_{\max}} r^3 \mathrm{e}^{-r/\bar{r}} \, \mathrm{d}r = r_0^3.$$

Naturally, for numerical purposes, the exponential law has to be discretized.

Nevertheless the current model gives interesting information concerning droplets repartition and expansion in the spray.

Acknowledgements

The experimental study and comparisons with computation was supported by SNECMA.

References

Adam, O., 1997. Etude expérimentale du comportement des gouttes en régime d'interaction. Thèse ENSAE.

Hsiang, L.P., Faeth, G.M., 1992. Near-limit drop deformation and secondary breakup. Int. J. Multiphase flow 18 (5), 635–652.

Hsiang, L.P., Faeth, G.M., 1993. Drop properties after secondary breakup. Int. J. Multiphase flow 19 (5), 721–735.

Hsiang, L.P., Faeth, G.M., 1995. Drop deformation and breakup due to shock wave and steady disturbance. Int. J. Multiphase flow 21, 545–560.

Krzeczkowski, S.A., 1980. Measurement of liquid droplet disintegration mechanisms. Int. J. Multiphase flow 6, 227–239.

Lenard, P., 1904. Über Regen. Meteorologische Zeitschrift 21, p. 249.

Nigmatulin, R.I., 1990. Dynamics of multiphase media. English Edition Editor, vols. 1,2.

Pilch, M., Erdman, C.A., 1987. Use of breakup time data and velocity history data to predict the maximum size of stable fragments for acceleration-induced breakup of liquid drop. Int. J. Multiphase flow 13 (6), 741–757.

Shraiber, A.A., Podvysotsky, A.M., Dubrovsky, V.V., 1996. Deformation and breakup of drops by aerodynamic forces. Atomization and Sprays 6, 667–692.

Wierzba, A., 1990. Deformation and breakup of liquid drops in a gas stream at nearly critical Weber numbers. Experiment in Fluids 9, 59–64.